Atomic-beam measurements of helium F-G, F-H, and F-I intervals

David R. Cok* and S. R. Lundeen
Lyman Laboratory of Physics, Harvard University, Cambridge, Massachusetts 02138
(Received 22 September 1980)

The fast-atomic-beam microwave-optical resonance technique has been used to measure the $8F$-$8G$, $8F$-$8H$, $7F$-$7H$, and $7F$-$7I$ intervals in helium. The electrostatic fine-structure intervals derived from these measurements and from theoretical values of the magnetic fine structure are $8F$-$8G$, 3898.525(0.041); $8G$-$8H$, 931.34(0.44); $7G$-$7H$, 1359.16(0.11); and $7H$-$7I$, 402.8(4.7) MHz. Additional theoretical work is needed to understand these intervals beyond the 1% level.

I. INTRODUCTION

The Rydberg states of helium have one highly excited electron bound to a hydrogenic core; thus a precise theoretical description approaching that obtained for one-electron systems should be possible. This is especially true of high-angular-momentum Rydberg states where there is little penetration of the ion core by the excited electron. Experimental knowledge of these states is derived largely from the work of Farley, MacAdam, and Wing who have measured a large number of D-F and D-G intervals using microwave-optical techniques.[1] Other experimental techniques have been used to study these states with less precision.[2,3] The theoretical description of these states lags considerably behind the experiments. The polarization model of Deutsch[4] gives the dipole and quadrupole corrections to the hydrogenic term values. Chang and Poe[5] have carried out a more precise calculation for D, F, and G states using a perturbation theory approach. There is agreement between experiment and theory for these electrostatic intervals only at the level of about 1%, while many of the intervals have been measured to 10 ppm.

The magnetic fine structure is given in lowest order by the expectation values of the magnetic operators over the hydrogenic wave functions.[6] Higher-order corrections have been treated by other authors.[7,8] The present authors have discussed an "extended adiabatic approximation" to the magnetic fine structure that improves agreement with experimental data in D states.[8] In higher-L states, deviations from hydrogenic magnetic structure have not yet been resolved experimentally.

The availability of precise experimental data in states above $L = 3$ will provide a test of improved theories of the electrostatic intervals that is less sensitive to overlap and correlation effects. If the theory of these intervals can be improved to the 0.1% level, it should be possible to test for the presence of a new type of two-electron radiative correction recently proposed by Kelsey and Spruch.[9] It may also be possible eventually to study the effects of black-body radiation on the dynamics and structure of these states.[10]

II. EXPERIMENTAL TECHNIQUE

The excited states of helium are studied here in a field-free, vacuum enviroment using the fast atomic beam microwave-optical technique. The apparatus is shown in Fig. 1. A commercial duoplasmatron ion source generates a 5–20-keV beam of He^+; this is focused through a windowless, differentially pumped charge-exchange cell containing a few hundred millitorr of argon. The fast neutral helium beam which results contains large numbers of high-L states (typically 10^8 $8F$/sec in a beam of a few microamps). The microwave interaction region which drives the F-G, F-H, or F-I transitions is a section of circular waveguide in which the guided waves travel either parallel or antiparallel to the atomic beam. There is a weak reflected wave in the waveguide which produces a small satellite line, shifted by the Doppler effect and well resolved from the dominant resonance. The nF population is detected by observing the fluorescence intensity of either the $4\,^1D$–$2\,^1P$ or $4\,^3D$–$2\,^3P$ line. The phototube and filter monitoring the optical line are about 500 nsec downstream from the charge-exchange cell. By this time all target-produced $4D$ states have decayed and the detected light is the result of cascade decays from nF states. Resonances are detected by measuring the modulation of the optical intensity

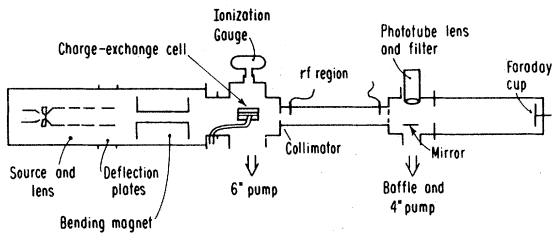

FIG. 1. The atomic beam apparatus.

as the microwave power is switched on and off. Resonance line shapes observed with this apparatus for the 8^1F_3–$^1G_4$ transition were analyzed in detail in a previous paper.[11] The experimental line widths (2 MHz) are determined primarily by the transit time through the interaction region.

III. 8F-G RESONANCES

The 8F and 8G manifolds, including magnetic structure, are shown in Fig. 2. In states with L greater than 2, the singlet and triplet states of the same L and J are strongly mixed; for G and higher states, the mixing is nearly complete and the designations "singlet" and "triplet" are used by convention to refer to the higher- and lower-energy states, respectively. There are eleven allowed electric-dipole transitions among these eight levels. One of these, the 8^3F_4–$^3G_3$, has a small matrix element and is too close to the 8^3F_4–$^3G_5$ to be observed when the latter is power broadened. The other ten transitions have all been resolved. Each was observed for both directions of propagation of the microwave fields with respect to the atomic beam (UP and DOWN), giving a total of 20 lines. All lines were observed with an He^+ beam energy of 13.0 KeV, at a microwave power level chosen to give about 50% saturation of each transition.

Resonance frequencies were obtained from the line scans in the following manner. Well-isolated lines could be fit directly to the line-shape theory developed in Ref. 11. The 8^1F_3–$^1G_4$ (up) line, which was thoroughly analyzed in Ref. 11, was not remeasured here; the line center obtained there is used here as well. Note that this one line was taken at 14.5 kV, whereas the others were at 13.0 kV. Some lines required special treatment because of nearby overlapping lines. In some cases the overlapping line was produced by the weak counter propagating reflected wave in the waveguide driving another allowed transition. All such cases are listed below as follows:

(a) 8^1F_3–$^3G_3$ (up), which was resolved but overlapped by 8^1F_3–$^1G_4$ (down).

(b) 8^3F_4–$^3G_4$ (down), which was resolved but overlapped by 8^3F_2–$^3G_3$ (down).

(c) 8^3F_4–$^3G_4$ (up), which was resolved but overlapped by 8^3F_2–$^3G_3$ (up) and (down).

(d) 8^3F_3–$^3G_4$ (down) and 8^3F_4–$^3G_5$ (down), which were not resolved.

(e) 8^3F_3–$^3G_4$ (up) and 8^3F_4–$^3G_5$ (up), which were not resolved.

Cases (a), (d), and (e) were fit by two lines simultaneously. In case (b) the interfering resonance was a fairly distant power-broadened line. An estimate of the line shape of the interfering resonance was obtained and subtracted from the data to give the desired line. The remainder was adequately fit by the usual one-transition line. The statistical error was increased to reflect the uncertainty in the estimate of the subtracted background. In case (c) the overlapping power-broadened resonances could not be satisfactorily removed, so no value is reported for this line. Figure 3 shows the observations and fit for the 8^1F_3–$^1G_4$ (up) resonance.

The line centers and statistical errors obtained from these fits are reported in Table I. Apart from the corrections discussed below, the average of the resonance frequencies for the two lines corresponding to a given transition is the best estimate of the transition frequency; half the

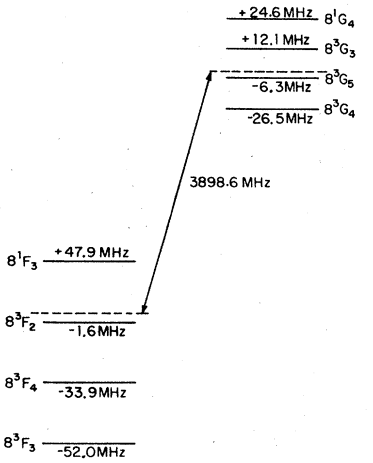

FIG. 2. The energy levels of the 8F and 8G manifolds.

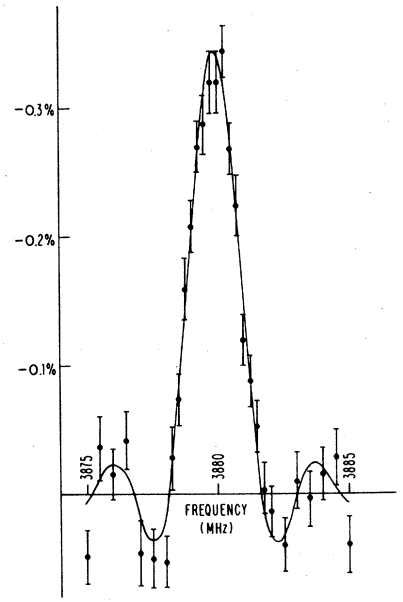

FIG. 3. The 8^1F_3–$^1G_4$ (up) resonance.

TABLE I. Results for the $8F$-G intervals (values in MHz).

	Measured value		Resonance	Doppler
	Up	Down	frequency	shift
$^1F_3$–$^3G_4$	3828.584(0.044)	3819.995(0.055)	3824.177(0.106)	4.286(0.059)
$^1F_3$–$^3G_3$	3867.724(0.175)	3858.522(0.058)	3862.930(0.140)	4.618(0.108)
$^1F_3$–$^1G_4$	3879.916(0.014)	3870.730(0.054)	3875.162(0.083)	4.468(0.055)
$^3F_4$–$^3G_4$		3901.732(0.140)	3906.067(0.228)	
$^3F_2$–$^3G_3$	3917.008(0.082)	3907.641(0.070)	3912.288(0.095)	4.684(0.074)
$^3F_3$–$^3G_4$	3928.909(0.190)	3919.671(0.210)	3924.254(0.162)	4.619(0.150)
$^3F_4$–$^3G_5$	3931.033(0.183)	3921.799(0.206)	3926.380(0.159)	4.617(0.147)
$^3F_4$–$^1G_4$	3961.535(0.062)	3951.625(0.046)	3956.687(0.159)	4.956(0.070)
$^3F_3$–$^3G_3$	3967.572(0.090)	3957.299(0.055)	3962.555(0.120)	5.138(0.081)
$^3F_3$–$^1G_4$	3980.090(0.060)	3970.110(0.078)	3975.165(0.137)	5.010(0.075)

difference between the two line centers gives the Doppler shift. The significant sources of systematic errors are discussed below and their numerical values are listed in Table II. The first two apply to each member of a Doppler pair individually; the last four apply only to the transition frequencies since they affect the two peaks equally.

A. ac Stark shift

The ac Stark shifts can be computed from first principles given a knowledge of the electric-field strength seen by the atoms. The calculated shifts include coupling of the resonant levels to all intermediate states in the $8D$, F, G, and H manifolds. The errors assigned to the corrections are 25% of the corrections, corresponding to the estimated uncertainty in the value of electric-field strength in the waveguide.

B. Beam-energy variations

There is a day-to-day uncertainty in the beam energy of 3%. The uncertainty in the beam velocity is then 1.5%, and the error to be assigned to a Doppler-shifted line is 1.5% of the Doppler shift.

C. Doppler shift

The frequency experienced by the atom is

$$f_{\text{atom}} = \gamma f_{\text{lab}} \mp \gamma\beta(f_{\text{lab}}^2 - f_c^2)^{1/2}.$$

If $f_{\text{av}} = (f_+ + f_-)/2$ and $f_{\text{diff}} = (f_+ - f_-)/2$, in which f_+ and f_- are the laboratory line centers for the two rf directions, then (neglecting insignificant terms),

$$f_{\text{diff}} = \beta(f_{\text{av}}^2 - f_c^2)^{1/2},$$

and

$$f_{\text{atom}} = f_{\text{av}} + f_{\text{av}}(2/\gamma - 1 - \gamma).$$

The correction indicated by the equation for f_{atom} in terms of f_{av} is then $[-0.925(0.086) \times 10^{-5}]f_{\text{av}}$, using the beam speed and error from the fit of the Doppler-shift data discussed below.

D. Unmodeled power shift

Using the data of Ref. 11 we placed an experimental limit of $-0.037(0.065)$ kHz/μV on any unmodeled power shift. This value and the diode voltage at which each transition was measured were used to estimate this error for each transition.

E. Ion current

Using additional data on the $8\,^1F_3$–$^1G_4$ transition, we placed experimental limits on any shift (such as a Stark shift) dependent on the ion current. For each line, the current during data taking was between 1.5 and 2μA. We assigned an error of 0.050 MHz for this effect.

F. Stark shifts

There are potential Stark shifts caused by the motional electric field. Because the magnetic field was not uniform along the center of the waveguide, it could not be completely nulled by external coils. The rms residual field of 0.21 G corresponds to a systematic uncertainty of 0.033 MHz in all lines.

The final values of the transition frequencies and Doppler shifts are listed in Table I. Note that the transition frequency for $8\,^1F_3$–$^1G_4$ is a weighted average of the centers of the two shifted lines since they were taken a different beam energies. Also we have a measurement of only one Doppler component of the $^3F_4$–$^3G_4$ line. The mean center for this line was obtained by computing the expected Doppler shift for this frequency given by the fit to the Doppler-shift data discussed below.

The values for f_{diff} obtained from the data can be fit to the equation for f_{diff} above to determine values for β and f_c. The data were adequately explained by the equation, although the test is not a stringent one since the data are close together in

TABLE II. Systematic errors applied to the $8F$-G measurements (values in MHz).

	ac Stark	Beam energy	Doppler shift	Power shift	Ion current	B field
$^1F_3$–$^3G_4$						
Up	−0.086(0.022)	(0.064)	−0.035(0.003)	(0.065)	(0.050)	(0.033)
Down	−0.070(0.018)	(0.064)				
$^1F_3$–$^3G_3$						
Up	−0.140(0.036)	(0.069)	−0.036(0.003)	(0.065)	(0.050)	(0.033)
Down	−0.175(0.044)	(0.069)				
$^1F_3$–$^1G_4$						
Up	0.000(0.000)	(0.072)	−0.036(0.003)	(0.005)	(0.050)	(0.033)
Down	0.000(0.000)	(0.068)				
$^3F_4$–$^3G_4$						
Up			−0.036(0.003)	(0.130)	(0.050)	(0.033)
Down	−0.319(0.080)	(0.070)				
$^3F_2$–$^3G_3$						
Up	0.000(0.000)	(0.071)	−0.036(0.003)	(0.005)	(0.050)	(0.033)
Down	0.000(0.000)	(0.071)				
$^3F_3$–$^3G_4$						
Up	0.000(0.000)	(0.072)	−0.036(0.003)	(0.005)	(0.050)	(0.033)
Down	0.000(0.000)	(0.072)				
$^3F_4$–$^3G_5$						
Up	0.000(0.000)	(0.072)	−0.036(0.003)	(0.005)	(0.050)	(0.033)
Down	0.000(0.000)	(0.072)				
$^3F_4$–$^1G_4$						
Up	+0.145(0.036)	(0.074)	−0.037(0.003)	(0.130)	(0.050)	(0.033)
Down	+0.144(0.036)	(0.074)				
$^3F_3$–$^3G_3$						
Up	+0.158(0.040)	(0.077)	−0.037(0.003)	(0.065)	(0.050)	(0.033)
Down	+0.156(0.039)	(0.077)				
$^3F_3$–$^1G_4$						
Up	+0.122(0.031)	(0.076)	−0.037(0.003)	(0.098)	(0.050)	(0.033)
Down	+0.083(0.022)	(0.076)				

frequency relative to the distance to f_c. Consequently, f_c is not well determined, but its value of 3419(108) MHz is not in disagreement with the value of 3459(138) MHz obtained from the waveguide radius [2.5(0.1) cm]. The fitted value of the velocity, 74.5(3.5) cm/μsec, is in satisfactory agreement (1.3 s.d.) with 79.2 cm/μsec, the speed of 13.0-kV helium atoms.

The line centers obtained in this work can be compared with values obtained from the $8D$-F and $8D$-G measurements reported in Ref. 1. The measurements are of approximately equal precision and are in excellent agreement. The mean difference between the two sets of results is -74(70) kHz and the chi-squared value for the hypothesis that there is no difference is 7.4 for 10 degrees of freedom. The details of this comparison are contained in Ref. 12.

From our results one can extract the electrostatic fine-structure interval and the F-state exchange energy. There are two parts to the calculation of the helium energy levels: the electrostatic intervals and the magnetic fine structure. The latter was treated by us previously.[8] In states with L larger than 2 the corrections to the hydrogenic model are insignificant compared to our measurement errors, so the simple hydrogenic model should predict the magnetic fine structure adequately. Accurate values of the electrostatic and exchange energies are more difficult to obtain; the existing calculations are discussed later in this paper. We have fit our results to the fine-structure theory using hydrogenic matrix elements, floating the F-G electrostatic interval and the F exchange energy but fixing the G exchange at 0 as its estimated value [0.04 MHz (Ref. 13)] is small enough that the resulting shifts in the energy levels are negligible. The fit shows both internal consistency and good agreement with theory; it yields 3898.525(0.041) MHz for the $8F$-G electrostatic interval and 24.366(0.058) MHz for the F exchange energy.

IV. MULTIPLE-QUANTUM RESONANCES

Of the allowed multiple-quantum transitions, only the $7\,^1F_3$–$^1H_5$, $7\,^3F_2$–$^3H_4$, $7\,^3F_3$–$^3H_5$, $7\,^3F_4$–$^3H_6$, $8\,^1F_3$–$^1H_5$, and $7\,^1F_3$–$^1I_6$ resonances were carefully

measured. Multiphoton transitions have some difficulties not associated with one-photon transitions. In particular the power shifts are generally large and can be predicted only if the absolute microwave electric field is accurately known, so it was desirable to measure this shift by taking line scans at a number of power levels. Also, for our experimental arrangement, the Doppler shifts added complications. At the frequencies of the two-photon transitions the reflected wave was appreciable. Since the signal size in two-photon transitions depends on the square of the rf power and since an atom picking up a photon from each direction can do so in two different orders (doubling its transition amplitude), the relative sizes of the peaks are 1, $4r$, and r^2, if r is the reflection coefficient. For rf propagating along the beam we saw an up-shifted and a nonshifted peak; for rf propagating counter to the beam we saw down-shifted and nonshifted peaks. Typically, the two observed peaks were roughly equal in size (cf. Fig. 4); the expected size of the third peak is then $\frac{1}{16}$ of the size of the other two. Including this small third peak in the line-shape fits did not significantly change the line centers. Furthermore, any systematic shift caused by this third peak would act in the opposite direction when the direction of rf propagation is reversed. Hence we believe that any error caused by ignoring this third peak is negligible.

For each of the transitions, line scans were taken in both rf directions at four to six power levels. The experimental configuration was the same as for the $8F$-G data except that an attenuator was placed before the power-monitoring diode to accommodate the increased power, and that the $8F$-H and $7F$-I transitions required a larger waveguide.

The data for each line scan were fit to a sum of Lorentzian lines plus a background. No attempt was made to develop a line-shape theory for the multiphoton lines. Since these transitions are below saturation and the signal-to-noise ratio is not large, Lorentzians explain the line shapes adequately. A flat background term is included to account for any off-resonance effects of very over-saturated single-photon lines. For the $^1F_3$–$^1H_5$ and $^3F_2$–$^3H_4$ lines, each fit had a shifted and a nonshifted component. The $^3F_4$–$^3H_6$ and $^3F_3$–$^3H_5$ lines are close enough that they had to be included together in one fit with four components. Figure 4 shows the data and fit for a medium power line scan of the $7\,^3F_2$–$^3H_4$ (up) resonance. To obtain the best estimates of the transition frequencies, all the data for a given transition were fit to an equation containing linear power shifts and a symmetrical Doppler shift. The power shifts were typically 1 MHz over the range of powers used for the two-photon lines. This equation adequately explained the data; the line centers obtained from these fits are listed in Table III with the error bars increased to account for the systematic errors discussed previously. The two-photon lifetime shift[14] is completely negligible here (10^{-5} of the linewidth).

Three-photon resonances are further complicated by the different power shifts of the magnetic sublevels. At the power levels required to drive the $7F$-I transition the power shifts are about 12 MHz and the differential shift is sufficient to broaden the resonance line. We have not yet resolved this substructure and consequently the error on this

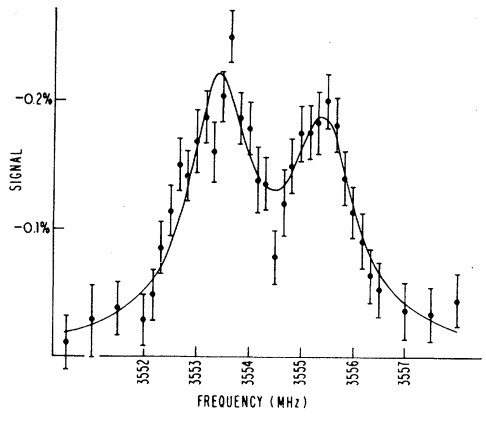

FIG. 4. A $7\,^1F_3$–$^1H_5$ (up) two-photon resonance fit to two Lorentzians plus constant background.

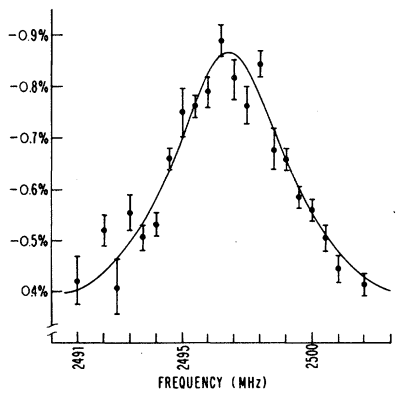

FIG. 5. A $7\,^1F_3$–$^1I_6$ (up) three-photon resonance fit to one Lorentzian plus constant background.

TABLE III. $7F$-H, $7F$-I, and $8F$-H results (values in MHz).

Interval	Measured frequency	Theoretical prediction [a]	Electrostatic interval
$7\,^1F_3$–$^1H_5$	3524.810(0.169)	$(A-45.379)/2$	7094.999(0.338)
$7\,^3F_2$–$^3H_4$	3553.160(0.082)	$(A+10.909)/2$	7095.411(0.164)
$7\,^3F_4$–$^3H_6$	3568.204(0.070)	$(A+41.258)/2$	7095.150(0.140)
$7\,^3F_3$–$^3H_5$	3572.659(0.079)	$(A+49.929)/2$	7095.389(0.158)
$8\,^1F_3$–$^1H_5$	2399.755(0.219)	$(B-31.350)/2$	4830.860(0.438)
$7\,^1F_3$–$^1I_6$	2481.92(1.58)	$(C-52.33)/3$	7498.08(4.75)

[a] A, B, and C are the relevant electrostatic intervals.

measurement is still quite large. The broad lines are adequately fit by a single Lorentzian plus background; Figure 5 shows the data and fit of a $7\,^1F_3$–$^1I_6$ line scan. As in the case of the two-photon lines, the data were fit to remove the power and Doppler shifts and the same systematic errors included to give the final result listed in Table III.

In order to obtain the electrostatic intervals from these measurements, we assumed hydrogenic magnetic structure and the F exchange values calculated from the data of Ref. 1.[12] The H and I exchange energies were set to zero. The one remaining parameter is the electrostatic splitting; a value for the parameter can be calculated from each measured interval as shown in Table III. For the $7F$-H interval we have four measurements of the electrostatic interval and these are seen to be in good agreement (the chi-squared value is 2.7 for 3 degrees of freedom). Our final value for the electrostatic $7F$-H splitting is then 7095.281 (0.085) MHz. Combining this with the $7F$-G splitting of 5736.123(0.072) MHz (Ref. 11) gives a $7G$-H interval of 1359.158(0.111) MHz. Using the value of the $8F$-G interval reported above and our measurement of 4830.86(0.44) for the $8F$-H interval, we obtain 931.34(0.44) MHz for the $8G$-H interval. Finally, the inferred value of the $7H$-I electrostatic interval is 402.8(4.7) MHz.

V. DISCUSSION OF RESULTS

Table IV summarizes the four electrostatic intervals measured here and compares them with the previous measurements of Refs. 1, 2, and 3. Also shown are theoretical estimates due to Deutsch[4] and Poe and Chang.[5] The comparison between theory and experiment is further illustrated in Fig. 6. Within the context of the polarization model, the binding energies of particular

TABLE IV. Electrostatic intervals in neutral helium (values in MHz).

	This work	Farley *et al.*	Beyer and Kollath	Panock *et al.*	Deutsch	Poe and Chang
$5F$-G					14142	
$6F$-G		8904.22(0.05)			8453	8742
$7F$-G		5736.12(0.07)			5424	5620
$8F$-G	3898.52(0.04)	3898.67(0.12)			3678	3859
$9F$-G		2765.26(0.06)	2724(173)	2722(105)	2604	2739
$10F$-G		2030.41(0.14)	1985(135)		1909	2010
$11F$-G		1533.68(0.24)			1440	1518
$6G$-H					2035	
$7G$-H	1359.16(0.11)		1437(38)		1332	
$8G$-H	931.34(0.44)		1011(43)		914	
$9G$-H			712(59)	695(64)	652	
$10G$-H			537(85)		481	
$7H$-I	402.8(4.7)		490(41)		409	
$8H$-I			332(56)		284	
$9H$-I			231(71)	213(77)	205	
$10H$-I			194(125)		152	
$8I$-K			282(81)		105	
$9I$-K			102(95)	84(77)	77	
$9K$-L				27(60)		

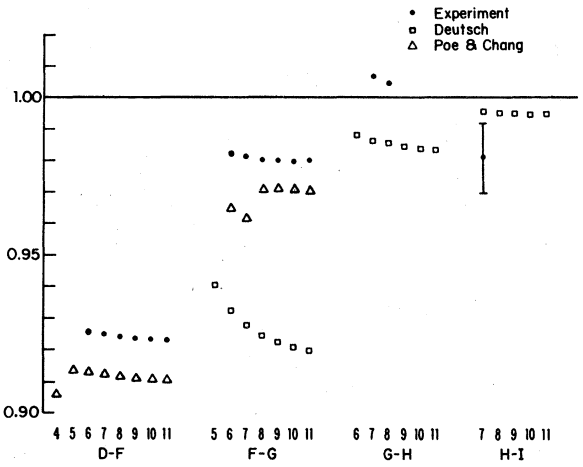

FIG. 6. The current experimental values (·), and theoretical calculations of Deutsch (Ref. 4) (□), Poe and Chang (Ref. 5) (△). All are normalized to the dipole polarization energy with $\alpha_d = \frac{9}{32}$ a.u.

Rydberg states are found by adding to the hydrogenic term values an adiabatic dipole polarization term of

$$V_{\text{dipole}} = -\tfrac{1}{2}\alpha_d \langle nL|\, r^{-4}\,|nL\rangle$$

with $\alpha_d = (9/32)$ a.u. In Fig. 6, both experimental and theoretical values for particular electrostatic intervals are shown normalized to transition energies derived from this term alone. The experimental values are from our analysis of Farley, MacAdam, and Wing's measurements (D-F and F-G) and the measurements reported here. These differ from the adiabatic dipole polarization term by -7.6%(D-F), -1.9%(F-G), +0.5(1)(G-H), and -1.9(1.1)%(H-I).

Deutsch[4] has added quadrupole terms to the polarization model (open squares in Fig. 6) but the data from F-G intervals suggest that the correction is too large by a factor of about 2. Other workers have confirmed the quadrupole term and derived additional terms in the asymptotic potential which are proportional to r^{-7} and to E/r^6 where E is the binding energy.[15] The expectation values of these additional terms is insufficient to account for the differences between experiment and the work of Deutsch. This may indicate the limitations of an approach to bound-state energies through the asymptotic potential.

A completely independent theoretical approach has been taken by Poe and Chang.[5] They have calculated the D-F and F-G intervals by perturbation theory, finding results which differ from experiment by 1–2%. Unfortunately, these calculations have not been carried beyond G states. To obtain higher accuracy, the nonrelativistic approach of Poe and Chang will need to be extended to include relativistic terms. For instance, the correction to the electron kinetic energy is $-P^4/8$ (to order α^2); this causes an energy shift of

$$\Delta E = \frac{3}{8}\frac{Z^4\alpha^2}{n^4} - \frac{Z^4\alpha^2}{n^3(2l+1)}$$

in hydrogenic states.[16] In the $7H$-I interval, this amounts to 14 MHz or 3% of the helium dipole polarization term. The importance of this and other single-electron relativistic terms increases relative to two-electron electrostatic effects as L increases.

Recently Kelsey and Spruch have proposed a "retardation correction" to the helium Rydberg energies.[9] This effect may be viewed as a new type of radiative correction, absent in one-electron systems, due to the correlation in the displacement of the two helium electrons by the fluctuating zero-point fields of the electromagnetic vacuum. Kelsey and Spruch give an expression for this effect:

$$\Delta E_{\text{retardation}} = \frac{11}{4\pi}\frac{\hbar e^2 \alpha_d}{mc}\,\langle nL\,|r^{-5}|\,nL\rangle\,,$$

valid for very high L states. The ratio of the expectation value of this term to the dipole polarization is 0.6% for the $7D$-F interval and 0.1% for the $7H$-I interval. Thus, existing experimental data are sufficiently precise to test for the presence of this term if other contributions to the intervals were understood at the 0.1% level.

ACKNOWLEDGMENTS

This research was performed with financial assistance from Research Corporation, the Harvard University Physics Department, and the National Science Foundation through NSF Grant No. 78-09657. Stephen Palfrey cooperated in taking the $8F$-H and $7F$-I data.

*Current address: Physics Division, Argonne National Laboratory, Argonne, Illinois 60439.

[1]John W. Farley, K. B. MacAdam, and W. H. Wing, Phys. Rev. A 20, 1754 (1979).

[2]H. J. Beyer and K. J. Kollath, J. Phys. B 11, 979 (1978).

[3]R. Panock *et al.*, Phys. Rev. A 22, 1050 (1980). (This group has in preparation measurements with errors of 10 MHz in manifolds other than $n = 9$.)

[4]C. Deutsch, Phys. Rev. A 13, 2311 (1976).

[5]T. N. Chang and R. T. Poe, Phys. Rev. A 14, 11 (1976);

10, 1981 (1974).
[6]H. Bethe and E. Salpeter, *Quantum Mechanics of One- and Two-Electron Atoms* (Springer, Berlin, 1957).
[7]R. M. Parish and R. W. Mires, Phys. Rev. A 4, 2145 (1971).
[8]David R. Cok and S. R. Lundeen, Phys. Rev. A 19, 1830 (1979).
[9]E. J. Kelsey and L. Spruch, Phys. Rev. A 18, 1055 (1978); 18, 845 (1978); 18, 15 (1978).
[10]T. F. Gallagher and W. E. Cooke, Phys. Rev. Lett. 42, 835 (1979).
[11]David R. Cok and S. R. Lundeen (unpublished).
[12]David R. Cok, Ph.D. thesis, Harvard University, 1980 (unpublished). The analysis uses data from Ref. 1.
[13]The value for 7G given in Ref. 5 scaled by $(\frac{7}{8})^3$ for 8G.
[14]D. A. Van Baak, B. O. Clark, and F. M. Pipkin, Phys. Rev. A 19, 787 (1979).
[15]R. J. Drachman, J. Phys. B 12, L699 (1979).
[16]E. U. Condon and G. H. Shortley, *The Theory of Atomic Spectra* (Cambridge University Press, Cambridge, 1951), p. 120.